

CFD MODELLING OF THE FLOW THROUGH A GRATE-KILN

B Reine GRANSTRÖM¹, T Staffan LUNDSTRÖM¹, B Daniel MARJAVAARA² and Simon TÖYRÄ²

¹ Luleå University of Technology, Division of Fluid Mechanics, 971 87 Luleå, SWEDEN

² LKAB, Box 952, 971 28 Luleå, SWEDEN

ABSTRACT

As part of an investigation regarding secondary reduction of NO_x emissions in a grate-kiln iron ore pelletizing plant, the aim of this specific research is to develop a CFD model that enhances the understanding of the aerodynamics and mixing of species inside the rotary kiln. At first, a parametric study of the pure airflow through the kiln is carried out and for certain conditions, a transient behaviour similar to that of vortex shedding was observed, with a dependence on momentum flux ratio between the secondary air jets. Further, the development of a preliminary coal combustion model is set out, which is in need of continued work in order to produce reliable predictions of various parameters relevant to the reduction process. However, the effect of the combustion on the flow field is limited, indicating that the pure airflow model can be used to broadly investigate the influence of the secondary air flow.

KEYWORDS: grate-kiln process, iron ore pelletizing, parallel jets, vortex shedding, coal combustion

INTRODUCTION

LKAB is an international high-tech minerals group, one of the world's leading producers of upgraded iron ore products for the steel industry and a growing supplier of industrial minerals products to other sectors. The company runs several pelletizing plants based on either the straight grate- or grate-kiln processes. In the grate-kiln process in focus in this paper, wet green pellets are loaded on a grate that takes the pellets through several zones for drying, pre-heating and oxidation from magnetite to hematite. Next, the pellets are fed into a rotary kiln where sintering takes place by heating, normally by a coal burner, to obtain the mechanical strength needed for further transport to the customer. Finally, the pellets pass through an annular cooler where heat is recovered by pre-heating ambient air being used in the process. The gas flow is thus in the opposite direction to the pellets and, in essence, the grate-kiln can be seen as a counterflow heat exchanger. A large amount of highly pre-heated air is supplied to the kiln for sufficient oxidation of magnetite pellets farther downstream in the grate. The large volume fraction of excess air in the combustion zone in combination with the relatively large increase in temperature results in a considerable production of nitrogen oxides (NO_x) (Smart *et al.*, 1999).

During the latest years, industry has faced increased governmental demands on control and reduction of pollutant emissions, one of which is NO_x (MÖD 2007:4). Consequently, LKAB is running several research projects with the objective to reduce NO_x emissions from their pellet production plants. One of these projects is to

investigate whether Selective Non-Catalytic Reduction (SNCR) is a suitable method for reducing NO_x emissions during the manufacturing of pellets. As part of this work, we here present the development of a numerical model that enhances the understanding of the aerodynamics and mixing of species inside the rotary kiln towards reliable predictions of crucial parameters for the SNCR process.

Computational Fluid Dynamics (CFD) is a useful tool that can provide insight into industrial applications where experimental measurements are difficult to carry out due to intricate geometries or harsh environments. Most of the previous work of applying CFD on rotary kilns is with application in the cement industry, however some attempts have been made for the iron ore pelletizing industry, e.g. Lundqvist *et al.* (2008). Ma *et al.* (2002) reported a model of the pure airflow through a rotary cement kiln. Furthermore, several attempts to simulate the reacting flow have been reported, see for example, Karki *et al.* (2000), Wang *et al.* (2006), and Ma *et al.* (2006). Principally, the focus has been on the overall behaviour of the cement kilns, but attempts have also been made to account for key phenomena such as the clinkerization reactions that take place in the solid bed (Mujumdar and Ranade, 2008). The *k-ε* model has been used exclusively to represent turbulence along with a Lagrangian description of the particle phase. The particle reaction model of previous works generally includes more or less advanced submodels for devolatilization and char oxidation as well as gas-phase combustion of the volatile matter. The computational grids used are relatively coarse, typically in the order of 18 000 – 600 000 elements. The focus of previous work has mostly been on optimising the production and the burner design, i.e. geometrical and operational parameters, and not explicitly on the secondary air flow pattern. Also, the kiln hoods of the previously studied cement kilns are of different type than the one of interest for this work. Consequently, it is necessary to perform a thorough study when applying CFD on this specific rotary kiln with its unique conditions and to, in detail, reveal the flow pattern.

In this work, using the commercial CFD package ANSYS CFX-11 (ANSYS® CFX, 2009), a full-scale model of the pure airflow through the rotary kiln is studied to acquire indications on the effect of the secondary air flow on the kiln aerodynamics. The reacting flow is also simulated, including devolatilization, char oxidation, combustion of volatile matter, thermal radiation and conjugate heat transfer. Incorporation of the coal combustion in the model enables examinations of the effect of the flame on the flow field and the suitability of the pure airflow model.

MODEL DESCRIPTION

Computational model overview

To start with, a simplified model of the pure airflow through the kiln is employed that is successively developed by taking combustion and other factors into account. Unless stated otherwise, model parameters are mutual for pure airflow and combustion simulations. The advection schemes used are *High Resolution* and *Specified Blend* = 1 for pure air flow and combustion simulations, respectively. Important processes that are neglected in this work are:

- the bed – the volume it occupies as well as its energy consumption due to the sintering process
- influence of downstream geometry, specifically the upward transition to the grate.

The rotation of the kiln is also neglected, but not considered to be a factor of significance. Further, important simplifications and assumptions are:

- simplified geometry of the secondary air channels and the burner
- inlet boundary conditions – typical volumetric flows are taken from process data and have not been varied.

Pure airflow model

The inlet cross-section of the pure airflow model can be seen in Figure 1.

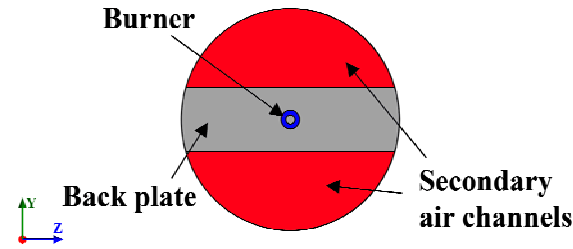


Figure 1: Geometry of the pure airflow model

The model consists of a section of the kiln, corresponding to about half its actual length. The coal burner is located at the end of the kiln, penetrating through the cross wall called *back plate*, which separates the upper and lower secondary air channels. In the model the burner is represented by airflow through an annular opening in the back plate, see Figure 1. This is called the primary air. The secondary air channels are simplified as identical half-circular surfaces. A structured computational grid with 1.56 million nodes was created with refinements close to the walls and the burner; see Figure 2. A strict grid independence study was performed with a finest grid of 4.66 million nodes, but the solutions did not appear to be within the asymptotic range and a Richardson extrapolation was not applicable. It will, however, later be shown that the overall flow in the model is the same regardless of the mesh used. The primary and secondary airs have identical properties but are treated as separate species so that respective air can be tracked down-stream the inlet. In order to obtain the correct density and the corresponding momentum of the air jets, the species are treated as ideal gases. Basic inlet boundary conditions are given in Table 1. The standard $k-\varepsilon$ model is used to model turbulence which result in two additional transport equations to solve in addition to the governing equations of mass, momentum and energy.

Parametric study

When the model is verified for one set of parameters the inclination and distribution between the secondary air channels are varied in a systematic manner. The inlet angles, α_1 and α_2 , are defined relative to the kiln centerline as shown in Figure 3, where M_1 and M_2 are fractions of the total airflow entering through the upper and lower channel, respectively.

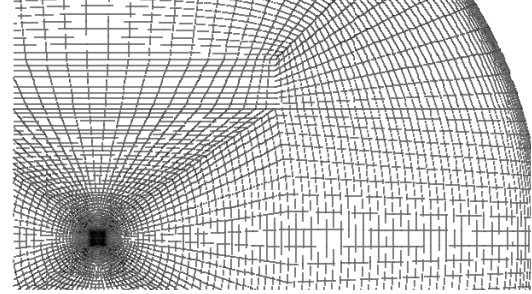


Figure 2: Computational grid for the pure airflow model

	Volumetric flow [Nm ³ /h]	Temperature [°C]
Primary air	8 000	60
Secondary air	200 000	1100

Table 1: Basic inlet boundary conditions

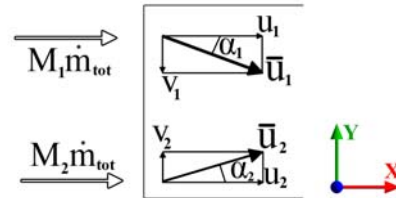


Figure 3: Secondary air channel inlets

As a measure to evaluate the impact of the jets emerging from each channel, the momentum flux is defined. Since the z -component of the inlet velocity is zero in all cases, each jet can be described in terms of the x and y -components of its momentum flux, given by:

$$J_x = \frac{(M_k \dot{m}_{tot})^2}{\rho A} \quad (1)$$

$$J_y = \frac{(M_k \dot{m}_{tot})^2}{\rho A} \tan \alpha_k, \quad (2)$$

where ρ is the air density, \dot{m}_{tot} is the total mass flow of the secondary air through both channels and A is the cross-sectional inlet area, which is equal for the channels. The 11 simulation set-ups are classified into three groups (A, B and C) based on the inlet angles, see Table 2.

Case	M_1	M_2	J_{x2}/J_{x1}	J_{y2}/J_{y1}
$\alpha_1=0^\circ, \alpha_2=0^\circ$				
A1	0.3	0.7	5.44	-
A2	0.4	0.6	2.25	-
A3	0.5	0.5	1.00	-
$\alpha_1=15^\circ, \alpha_2=15^\circ$				
B1	0.3	0.7	5.44	5.44
B2	0.4	0.6	2.25	2.25
B3	0.5	0.5	1.00	1.00
$\alpha_1=15^\circ, \alpha_2=40^\circ$				
C1	0.3	0.7	5.44	17.05
C2	0.4	0.6	2.25	7.05
C3	0.5	0.5	1.00	3.13
C4	0.6	0.4	0.44	1.39
C5	0.7	0.3	0.18	0.58

Table 2: Data for the parametric study

In all cases given in Table 2, the simulations are first run in a steady state mode followed by a transient run in order to detect any transient effects. An important variable in the transient simulations is the Courant number, given in its one dimensional form by:

$$Co = \frac{u\Delta t}{\Delta x}, \quad (3)$$

where u is the fluid velocity, Δt is the time step and Δx is the grid size. Due to the considerable CPU time required for the transient simulations, the time step is chosen to obtain convergence within 10 coefficient loop iterations, which is considered fulfilled when maximum residuals are below $5e-4$ and equation imbalances are below 1%; this gives $Co_{RMS} < 5$ and $Co_{MAX} < 25$. Since the code is implicit, small Co s are generally not required for stability; this is problem dependent though (ANSYS® CFX, 2009). To assure that the transient behaviour is captured, simulations with time steps corresponding to $Co_{RMS} < 1$ were also carried out without any noticeable difference in behaviour of the flow and therefore the Co s obtained are considered low enough.

Preliminary combustion model

Particle transport

The pulverized coal is represented by a finite number of particles whose motion is computed in a Lagrangian frame of reference. Each particle is tracked through the flow field and represents a sample of particles that follow an identical path, i.e. a particle trajectory. The interaction between the dispersed and continuous phases is two-way coupled with appropriate particle source terms included in the transport equations. The various forces acting on a particle dispersed in a continuous fluid include those due to drag, pressure gradient, gravity, turbulent dispersion etc. In the present work, only the drag force and buoyancy force due to gravity are accounted for. The aerodynamic drag force on a particle is given by

$$F_D = \frac{1}{2} C_D \rho_f A_p |u_f - u_p| (u_f - u_p), \quad (4)$$

where A_p is the effective particle cross-sectional area and indices f and p denote the fluid and the particle phase, respectively. C_D is the drag coefficient and is calculated by a modification of the drag model of Schiller and Naumann (1933),

$$C_D = \max\left(\frac{24}{Re} \left(1 + 0.15 Re^{0.687}\right) 0.44\right), \quad (5)$$

Particle reaction model

In addition to the particle forces, appropriate source terms are included in the transport equations to account for heat release, consumption of O_2 and production of CO_2 and H_2O due to the combustion reactions. The coal combustion is modelled by three processes; devolatilization, char oxidation and combustion of volatile matter. The devolatilization is modelled using a single reaction model where raw coal is decomposed into char while volatile gases are released from the particle. In the present model, the volatile yield is obtained by multiplying the proximate yield with a factor 1.25. The total amount of material released during the devolatilization is the actual volatile yield along with the moisture in the fuel. The relative amounts of carbon, hydrogen and oxygen in the volatiles are calculated based on the ultimate analysis, which in turn determines the stoichiometric coefficients in the gas-phase combustion

reactions involving the volatiles. The devolatilization rate is calculated by an Arrhenius type expression on the form:

$$k_v = A_v \exp\left(-\frac{E_v}{RT_p}\right), \quad (6)$$

where T_p is the particle temperature and A_v and E_v are a pseudo frequency factor and a pseudo activation energy, respectively. The following oxidation of the remaining char is described using a model that is controlled by external diffusion of oxygen to the particle and kinetics of the oxidation reaction. The overall char reaction rate is controlled by the smaller of the rates of diffusion, k_d , and oxidation, k_c , and is given by:

$$\left(k_d^{-1} + k_c^{-1}\right)^{-1} N_{O_2} 4\pi R_p^2 \frac{P}{P_A}, \quad (7)$$

where N_{O_2} is the molar fraction of O_2 in the gas, R_p is the particle radius, P_A is the atmospheric pressure and P is the local pressure. The rates are calculated as follows:

$$k_d = \frac{D_{ref}}{R_p} \left(\frac{T_p + T_g}{2T_{ref}}\right)^\beta \frac{P_A}{P} \quad (8)$$

$$k_c = A_c \exp\left(-\frac{T_c}{T_p}\right), \quad (9)$$

where T_p is the particle temperature, T_g is the far-field gas temperature and T_{ref} is the reference temperature, which is 293K. The dynamic diffusivity D_{ref} is set to $1.8e-5$ kg/ms and the exponent β is set to 0.75. The parameters A_c and T_c are set to 497 kg/m²s and 8540K, respectively. (ANSYS® CFX, 2009)

Gas-phase combustion

The combustion of the released volatiles is represented by the eddy dissipation model (ANSYS® CFX, 2009). There is no kinetic control of the combustion process; instead the reaction rate is controlled by the mixing of reactants. The rate is assumed to be inversely proportional to a mixing time defined by the ratio of the turbulent kinetic energy, k , and the dissipation rate of k , ε .

Simulation setup

In contrast to the pure airflow model, the full length of the kiln is modelled, including an expansion of the diameter after about half its length. The geometry of the coal channel and secondary air channels are unchanged, but an annular air channel with swirl vanes is added concentrically within the coal channel, see Figure 4.

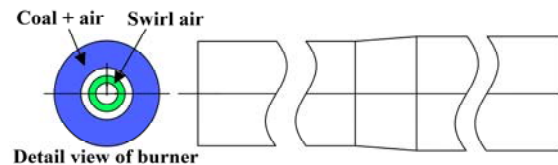


Figure 4: Geometry of the combustion model

A structured computational grid consisting of 1.13 million nodes is created for the combustion geometry, similar to the pure airflow grid but coarser. Due to extensive computational requirements this relatively coarse grid is considered acceptable as a base for further work, in which

the grid will be refined. As compared to previous work the grid is fine or finer, see for example Ma *et al.* (2006) or Mujumdar and Ranade (2008). The volumetric flow through the swirl channel is 750 Nm³/h at 60°C, with a tangential component approximated by a 30° swirl. Otherwise, the volumetric flows are unchanged but the air at the inlets is now defined as a mixture of O₂ and N₂. The volume fractions are set to 19 % and 81 %, respectively, to match the limited oxidation that takes place in the cooler. Coal particles are introduced through the coal channel with a velocity equal to the airflow. The coal mass flow is 1.75 kg/s, represented by 1,000 particle trajectories. A Rosin-Rammler distribution is used to specify the particle sizes, in which the mass fraction R above diameter d is given by:

$$R = e^{-\left(\frac{d}{d_e}\right)^\gamma}, \quad (10)$$

where γ is a spreading parameter and d_e is a fineness measure defined as the diameter for which $R = 0.368$ (ANSYS® CFX, 2009). The Rosin-Rammler parameters are chosen to fit a sieving analysis of the coal used in the plant. Properties of the coal used in the simulations are based on a proximate and ultimate analysis of the actual coal. The temperature of both the continuous and the particle phase is in these simulations limited to 2600 K.

RESULTS AND DISCUSSION

First the results for the pure airflow simulations will be presented followed by those with combustion added.

Pure airflow model

As mentioned, a strict grid independence check was not achieved. However, when comparing the predicted mixing for different grids the variation is small and the 1.56 million-node grid is considered sufficient to broadly predict the flow, see Figure 5. Complete mixing of primary and secondary air would correspond to a uniform primary mass fraction 0.038.

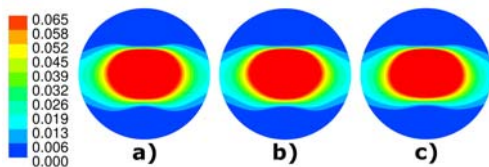


Figure 5a-c: Contour plots of primary air mass fraction at outlet of case A1 for grids a) 1.56, b) 2.75 and c) 4.66 million nodes

The results from the simulations indicate that the flow is strongly dependent on the ratio of momentum flux between the two secondary air jets. For all cases in group A, the component of J_i in the y -direction, see Eq. (2), is zero. When the momentum flux of one of the jets is dominating in magnitude, so that the ratio J_{x2}/J_{x1} is considerably larger or smaller than unity, the flow is steady and the weaker jet is entrained by the dominating one. As the magnitude of the dominating jet is decreased, the merge point between the jets moves towards the weaker jet and the extension of the wake behind the back plate increases somewhat, see Figure 6a-b. As the ratio approaches unity the flow becomes transient, characterized by a periodic flapping motion similar to that seen in vortex shedding behind a bluff body. This is illustrated by the instantaneous streamlines in Figure 6c; the motion is sinuate with a period of about 0.37 s and the

merge point moves periodically in the vertical direction. The amplitude of the oscillations peaks at the matched momentum flux seen in Figure 6c; in the parametric study overall, this is the extreme case with strongest oscillations. Similar trends have been reported for experiments on plane parallel jets by Anderson *et al.* (2003) and Bunderson and Smith (2005). Preliminary results of PIV experiments on a scaled down water model of another of LKAB's kilns has also shown similar behaviour as shown in Figure 6c (Larsson *et al.*, 2009).

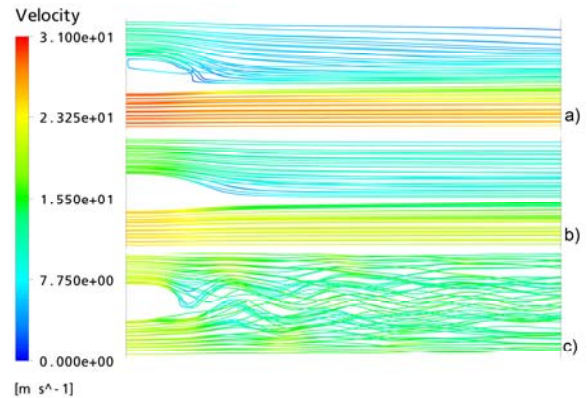


Figure 6a-c: Sec. air streamlines for case A1, A2 and A3

Notice that, since buoyancy is not modelled, Figure 6a-b can be vertically reversed to give a mirrored distribution.

The behaviour is similar in the corresponding cases of group B, with transient effects predicted in case B3. The amplitudes of the oscillations are however somewhat decreased and the period is shorter, about 0.26 s. Compared to group A, the wake behind the back plate decreases since the jets are inclined towards each other.

In case C1, the total momentum flux of jet 2 is sufficient to effectively penetrate jet 1 and force it upward rather than entraining it, see Figure 7a.

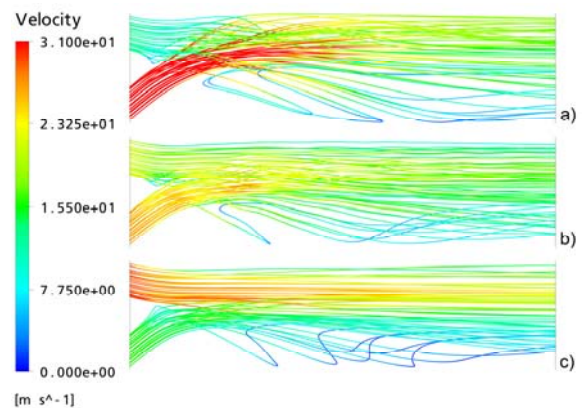


Figure 7a-c: Sec. air streamlines for case C1, C3 and C5

Comparing to case C2 the trend is similar to previous findings; the wake behind the back plate increases as the x - and y -momentum ratios simultaneously decreases. The dependence on the x -momentum flux ratio is similar to the previous groups but the aspect of unmatched y -momentum flux is also shown to have an influence on the flow. Case C3, with matched momentum flux in x - but not y -direction, shows oscillations similar to the corresponding distributions of group A and B.

For case C4 however, jet 2 is dominating for the x -momentum flux while jet 1 is dominating for the y -momentum flux resulting in an oscillating flow field similar to case C3. The trend differs from case A2, B2 and C2 that have the same ratio in x -direction as case C4, but steady flows. The amplitudes of the oscillations are smaller than for case A3 and B3, with periods of 0.19 and 0.16 s for case C3 and C4, respectively. For case C5, jet 2 hardly penetrates jet 1 despite its upward inclination. When the jets meet, jet 2 is somewhat straightened out and is, in essence, entrained by jet 1.

For the steady cases of group A and B, the primary air stream is more or less flattened as it is constricted by the secondary air jets, which can be seen from the contour plots in Figure 8. For the steady cases A1-2 and B1-2, the dilution of primary air is slightly increased with increasing x -momentum flux ratio. The oscillations in cases A3 and B3 give a significant increase in the mixing as illustrated in Figure 8. In these cases, the secondary air jets are entrained by each other and the flow encircles the primary air jet. Consequently, primary air from the lateral edges of the jet is entrained periodically upwards and downwards, resulting in the profiles seen in the time averaged plots. For all cases in group C, a similar entrainment behaviour is predicted where a swirling flow is established above the primary air jet, similar to a wake. This is indicated in Figure 8, where the profiles show a concentration of primary air above the lateral edges of the primary air stream. However, for C5, jet 1 is strongly dominant implying that the primary air hardly spreads over the uppermost part of the cross-section.

Preliminary combustion model

Combustion simulations are carried out for the inlet boundary conditions of case C5, see Table 2. It should be pointed out that this case is an extreme and cannot be seen as a representative for the other cases. Focus is here set on the flow field and how it is affected by the combustion while discussion of temperature and species concentration fields etc. are left for future studies.

The predicted flow field is similar to the pure airflow; the propagation of the secondary air jets are somewhat distorted by the flame, but not affected to any larger extent, see Figure 9. The most noticeable effect of the incorporation of combustion on the velocity field is the volumetric expansion and appertaining velocity increase of the gas due to the heat release. After the flame ignites shortly downstream of the burner, the gas begins to expand with a subsequent increase in velocity. However, this expansion has no drastic effect on the secondary air jets, whose directions remain similar to the corresponding pure airflow case, see Figure 9. The increase in velocity due to the combustion takes place mainly below the dominating upper jet, and the low-velocity region in the lower part of the kiln decreases compared to the pure airflow. Naturally, the volumetric expansion is largest in and around the flame zone where the increase in temperature is largest; however, all gas inside the kiln is heated by the flame and a general velocity increase is thus seen over the whole cross-section.

Outside of the flame zone, in the regions farther sideways towards the periphery, the distortion of the flow field due to the combustion is even less and the main difference compared to the pure air flow is that the overall velocity increases farther downstream. This can be seen in Figure 10, which shows velocity vectors projected on an x - y plane

displaced 2 m from the centerline in the z -direction. As the flame zone is constricted by the secondary air jets, it expands laterally rather than vertically, which is indicated by the velocity field on the diametrical x - z plane in Figure 11 compared to Figure 9.

Also, similar to what was described for the corresponding pure air flow case, as the upward secondary air jet meets the flame zone it encircles the flame creating a swirling flow on the upper side, see Figure 12.

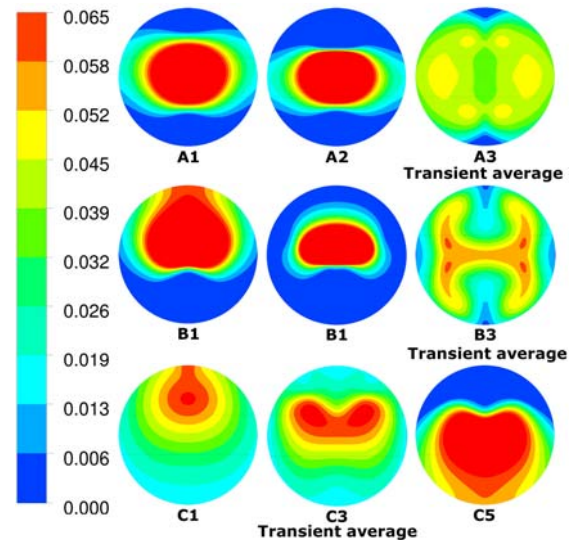


Figure 8: Contour plots of primary air mass fraction at outlet for selected simulation cases

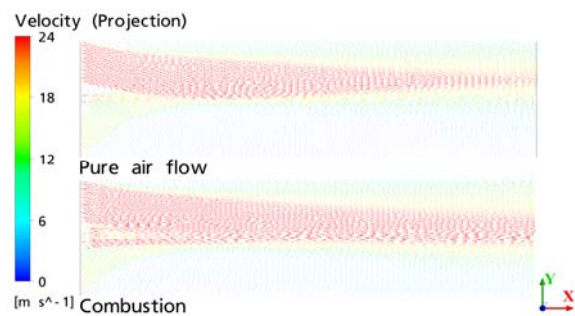


Figure 9: Vector field projected on diametrical x - y plane

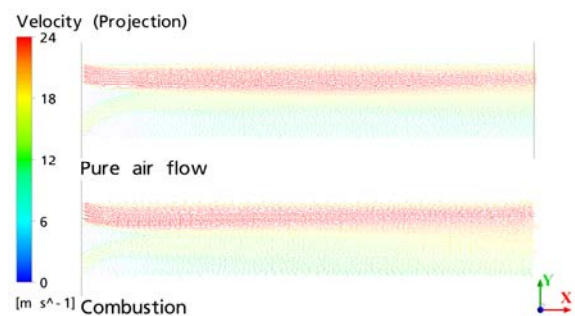


Figure 10: Vector field at x - y plane at $z=2$ m

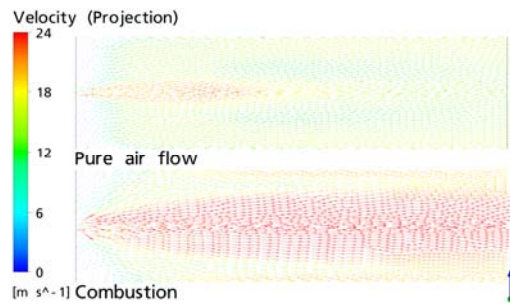


Figure 11: Vector field projected on diametrical x-z plane

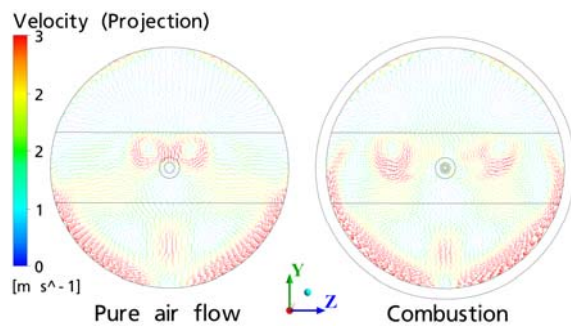


Figure 12: Vector field projected on a y-z plane at x=5 m

Both with and without combustion, there is a swirling flow in the lower part of the cross-section that meets the swirling flow above the flame. Since the flame mainly expands laterally, the vortices are displaced closer to the periphery compared to the pure air airflow. Also, there is a larger flow of gas along the kiln wall, going from the upper vortices to below the flame zone.

CONCLUSION

A full-scale CFD model of pure airflow through the rotary kiln was developed, on which a parametric study was carried out varying the inclination of and distribution between the secondary air channels. The predicted kiln aerodynamics was strongly dependent on the ratio of momentum flux in the x- and y-directions (axial and vertical) of the two secondary air jets. For ratios considerably larger or smaller than unity, the flow was steady and the weaker jet was entrained by the dominating one, with a stronger entrainment for ratios far from unity. However, for matched momentum flux the flow oscillated behind the back plate like vortex shedding behind a bluff body. Preliminary results of PIV measurements on a scale model having essentially the same geometry confirm this behaviour. Anyway the mixing is considerably improved by the oscillation.

A preliminary combustion model is developed by incorporating the pulverized coal using a Lagrangian description with devolatilization and char oxidation along with gas-phase combustion of the released volatiles. A main result is that the effect on the flow field from the combustion is small. This indicates that the pure airflow model could be used to broadly investigate how the secondary air flow influences the kiln aerodynamics and mixing of species. It also provides justification to the use of water scale models in which the volumetric expansion of the flame cannot be accounted for.

ACKNOWLEDGEMENTS

This work was carried out within the framework of the Faste Laboratory, a VINNOVA Excellence centre.

REFERENCES

- ANDERSON, E.A., SNYDER, D.O., CHRISTENSEN, J., 2003, "Periodic flow between low aspect ratio parallel jets", *Journal of Fluids Engineering, Transactions of the ASME*, **125**, 389-392.
- ANSYS® CFX, 2009, Release 11.0, Help System, ANSYS CFX-Solver Theory Guide, ANSYS, Inc.
- SMART, J.P., JENKINS, B.G., VAN DE KAMP, W.L., (1999), "Investigation into NO_x emissions from the high-temperature rotary cement kiln", *Journal of the Institute of Energy*, **72**, 99-109.
- BUNDERSON, N.E. and SMITH, B.L., 2005, "Passive mixing control of plane parallel jets", *Experiments in Fluids*, **39**, 66-74.
- KARKI, K.C., PATANKAR, S.V. and GRANT, J., 2000, "Simulation of Fluid Flow, Combustion, and Heat Transfer in a Coal-Fired Cement Kiln", *American Society of Mechanical Engineers, Fuels and Combustion Technologies Division FACT*, **23**, 103-111.
- LARSSON, I.A.S., LINDMARK, E.M., LUNDSTRÖM, T.S., MARJAVAARA, B.D. and TÖYRÄ, S., 2009 "Kiln aerodynamics - Visualisation of merging flow by usage of PIV and CFD", *Proceedings of the Seventh International Conference on CFD in the Minerals and Process Industries*, Melbourne
- LUNDQVIST, M., SJÖSTRÖM, U. and MARJAVAARA, B.D., 2008, "Modelling heat transfer in the KK2 Coal Powder Fired Rotary Kiln Furnace at LKAB", *Computational Modelling in Minerals Processing 08*, Cape Town.
- MA, A., ZHOU, J. and LI, W., 2002, "CFD prediction of cold airflow field for multi-air channel pulverized coal burner in rotary kiln", *Proceedings of the Intersociety Energy Conversion Engineering Conference*, 418-421.
- MA, A.-C., ZHOU, J.-M., OU, J.-P. and LI, W.-X., 2006, "CFD prediction of physical field for multi-air channel pulverized coal burner in rotary kiln", *Journal of Central South University of Technology (English Edition)*, **13**, 75-79.
- MUJUMDAR, K.S. and RANADE, V.V., 2008, "CFD modeling of rotary cement kilns", *Asia-Pacific Journal of Chemical Engineering*, **3**, 106-118.
- MÖD 2007:4, Swedish Environmental Court of Appeal, case number M9927-05, <http://www.rattsinfosok.dom.se>
- SCHILLER, L. and NAUMANN, A., 1933, "Über die grundlegenden berechnungen bei der schwerkraftaufbereitung", *Vereines Deutscher Ingenieure*, **77**, 318-320.
- WANG, S., LU, J., LI, W., LI, J. and HU, Z., 2006, "Modeling of pulverized coal combustion in cement rotary kiln", *Energy and Fuels*, **20**, 2350-2356.